macromol

MDPI

Article

Polyethylene Oxide Hydrogels Crosslinked by Peroxide for the Controlled Release of Proteins

Aristeidis Papagiannopoulos [1,*], Eleni Vlassi [1,*], Stergios Pispas [1], Constantinos Tsitsilianis [2] and Aurel Radulescu [3]

[1] Theoretical and Physical Chemistry Institute, National Hellenic Research Foundation, 48 Vassileos Constantinou Avenue, 11635 Athens, Greece; pispas@eie.gr
[2] Department of Chemical Engineering, University of Patras, 26504 Patras, Greece; ct@chemeng.upatras.gr
[3] Jülich Centre for Neutron Science JCNS Forschungszentrum Jülich GmbH, Outstation at Heinz Maier-Leibnitz Zentrum (MLZ), Lichtenbergstraße 1, 85747 Garching, Germany; a.radulescu@fz-juelich.de
* Correspondence: apapagiannopoulos@eie.gr (A.P.); evlassi@eie.gr (E.V.)

Received: 2 December 2020; Accepted: 18 December 2020; Published: 22 December 2020

Abstract: Crosslinking of polyethylene oxide (PEO) using a peroxide in the melt is employed to synthesize soft hydrogels with the ability of controlled release of proteins. The viscoelastic properties of the swollen networks confirm the elastic nature of the synthesized material and they are in agreement with swelling characteristics. The hydrogels have mesh sizes at the nm scale as it is estimated by swelling measurements and measured by small angle neutron scattering (SANS). Diffusion of bovine serum albumin (BSA) and lysozyme (LYZ) out of the hydrogels is restricted by the presence of the network. The diffusion coefficient in the hydrogels is lower for BSA in comparison to LYZ, while in both cases it drops as the mesh size of the network becomes smaller. This study introduces the use of peroxide-crosslinked PEO networks in the investigation of protein transport within hydrogels, the development of hydrogel-based protein delivery patches and polymeric constructs.

Keywords: small angle neutron scattering; diffusion; mesh-size; network; rheology

1. Introduction

Polyethylene oxide (PEO) hydrogels have been established as biocompatible materials for applications in wound healing, drug delivery, and tissue engineering [1]. While PEO offers structural integrity, hydrophilicity, and ability to combine in copolymers with other functional polymers [2], it is nontoxic and biologically inert [3,4]. The control over architecture and mechanical properties of synthetic PEO hydrogels allows investigations of the role of scaffold elasticity on cell differentiation and proliferation [5] while their biodegradability and tissue adhesion properties may lead to promising wound sealants [6]. PEO can be combined with other polymers to create multifunctional systems as for example using heparin–peptide interactions for the formation of bioactive noncovalent networks [7] and carboxymethyl cellulose to make hydrogel films with potential in tissue engineering [8].

Crosslinking with the use of peroxides offers the possibility for reaction in the melt state by thermal decomposition, production of free radicals, and subsequent hydrogen abstraction from the polymer [9]. It has been successfully used to improve the processing and mechanical properties in bioplastics [10] and traditional polymers [11] and to synthesize branched vinyl polymers [12]. Peroxides have been also used to crosslink PEO in the melt and produce water-swellable hydrogels [13,14]. Controlled transport of biomolecules within hydrogels is crucial as it defines whether sustained administration e.g., for tissue regeneration applications [15] or acute release e.g., for the delivery anti-inflammatory agents [16] will occur. Therefore, versatile crosslinking procedures are very important for the development of novel multifunctional platforms for the investigation of loading and release of biomacromolecules.

In this work we use 2,5-bis(tert-butylperoxy)-2,5-dimethylhexane under thermal decomposition conditions to crosslink PEO in the melt in order to synthesize hydrogels with tunable mechanical and morphological properties for applications in protein and drug delivery. Swelling measurements are performed to estimate the mesh size and modulus of the swollen networks while these findings are supported by small angle neutron scattering (SANS) and rheology experiments. The release of globular proteins from the hydrogels is compatible with the morphological characteristics of the networks at the nanoscale. The prepared PEO hydrogels can be used as templates for transport of bioactive macromolecular substances.

2. Experimental

2.1. Materials

Poly(ethylene oxide) (PEO) with average molar mass (M_n) 5,000,000 $gmol^{-1}$, 2,5-bis(tert-butylperoxy) -2,5-dimethylhexane (Luperox 101), acetone (≥99.5%), dimethylformamide (DMF), and butanol (BUT) were purchased from Sigma-Aldrich (Athens, Greece) and were used without further purification. Bovine serum albumin (BSA) and lysozyme from chicken egg white (LYZ) were also purchased from Sigma-Aldrich (Athens, Greece).

2.2. Hydrogel Synthesis and Preparation

Based on the procedure put forward by Emami et al. [13] 500 mg of PEO were mixed with 1 mL of organic solvent/Luperox mixture. The final mixtures were placed at 85 °C for 15 min to become homogeneous and the temperature was raised to 160 °C for another 15 min for the crosslinking reaction to take place. In our case other solvents, i.e., butanol and DMF, were also used apart from acetone which was originally proposed [13]. Three different peroxide/organic solvent volume ratios were used for each solvent as shown in Table 1.

Table 1. Peroxide/solvent mixtures used for the synthesis of the polyethylene oxide (PEO) hydrogels for acetone (AC), butanol (BUT) and dimethylformamide (DMF) solvent.

Sample	% *v/v* Peroxide	Solvent
AC1	15	Acetone
AC2	30	
AC3	45	
BUT1	15	Butanol
BUT2	30	
BUT3	45	
DMF1	15	Dimethyl-formamide
DMF2	30	
DMF3	45	

Hydrogels were immersed in excess amount of water for swelling for three days while excess water was changed three times to wash uncrosslinked chains and remaining organic solvents/crosslinker.

2.3. Fourier Transform Infrared Spectroscopy

A Bruker Equinox 55 Fourier Transform Instrument was used to record the infrared spectra (FTIR). It was equipped with an attenuated total reflectance (ATR) diamond accessory (SENS-IR) and a press. Small pieces of swollen and washed hydrogels were placed at the center of the sample holding device, were dried under nitrogen stream and 64 scans were collected in the wavenumber range 500–5000 cm^{-1}, at 2 cm^{-1} resolution. Three measurements on different loaded samples were performed to confirm reproducibility.

2.4. Swelling Measurements

Hydrogel samples were equilibrated in distilled water at room temperature for 24 h. The mass of the swollen networks (m_s) was extracted by weighing the samples after removing excess solvent superficially with filter paper. Subsequently the hydrogel samples were placed in a vacuum oven for about one week under vacuum (at room temperature) and were weighed immediately after they were removed from the oven to obtain their dry mass (m_d). The swelling ratio was extracted by Equation (1). All experiments were run in triplicate.

$$r_s = \frac{m_s - m_d}{m_d} \times 100 \quad (1)$$

2.5. Small Angle Neutron Scattering

Small angle neutron scattering (SANS) was performed on the KWS-2 high intensity/wide-q small angle neutron scattering diffractometer, at the Jülich Centre for Neutron Science (reactor FRM II). The scattering vector (q) range was 0.002–0.1 $Å^{-1}$ and was covered by three separate detection configurations (2, 8, and 20 m detection length) with neutron wavelength λ = 4.5 Å. 2-D raw data were reduced by standard methodology and the reduced 2-D raw data that were isotropic were azimuthally integrated into 1-D scattered intensity $I(q)$. Numerically calculated model intensities used to fit the experimental data are convoluted [17] with a Gaussian function so that instrumental resolution is taken into account [18,19].

2.6. Rheometry

Rheological measurements were performed using a stress-controlled rheometer AR-2000 ex (TA Instruments), equipped with a plate-on-plate geometry (diameter = 20 mm). Dynamic oscillatory frequency sweep tests were carried out on the swollen hydrogels at strain amplitude 1% which was well inside the linear response. The linear response regime was estimated by oscillatory strain sweeps at constant frequency 1 Hz. Measurements were performed at 25 °C with the aid of a Peltier control system. A solvent trap was used to minimize water evaporation.

2.7. Loading and Release of Proteins

BSA and LYZ solutions of 20 mg·mL^{-1} concentration were prepared by dissolving protein powders in distilled water (pH 6.5) and allowing to equilibrate for 24 h at 4 °C. Swollen hydrogels were incubated in 10 mL protein solutions and kept at 4 °C for 144 h to equilibrate. Protein solution-swollen hydrogels of disc shape (1 mm in height and 8 mm in diameter) were cut with a biopsy punch, washed with distilled water to remove protein solution from their surface, and were immersed in 10 mL of distilled water at 25 °C. Aliquots of 1 mL from the solution were taken at predetermined time intervals and protein concentration was determined by UV-vis absorption at 280 nm. The aliquots were returned to the sample vial after UV-vis measurement. Experiments were run in triplicate. Calibration curves for BSA and LYZ were constructed using solutions of proteins with known concentration.

2.8. UV-Vis Absorption Measurements

UV–vis absorption spectroscopy was carried out on a UV–vis-NIR spectrophotometer Perkin-Elmer (Lamda 19) using an 1-cm-long quartz cuvette to load the samples. The absorbance at 280 nm was recorded for the quantification of protein concentration.

3. Results and Discussion

The crosslinking reaction was evaluated by FTIR experiments on PEO powder (before crosslinking) and on hydrogels that were previously washed and subsequently dried under nitrogen. The characteristic bands (Figure 1) that are found in the PEO powder are the CH bending at 1465, 1360, and 1343 cm^{-1},

the C–O stretching at 1279, 1249, and 959 cm^{-1}, the C-O-C stretching at 1095 cm^{-1}, and the CH_2 rocking at 842 cm^{-1}. In the crosslinked PEO the bands appear broader. The new characteristic band at 1720 cm^{-1} is related to C=O stretching of ester groups formed during the crosslinking reaction.

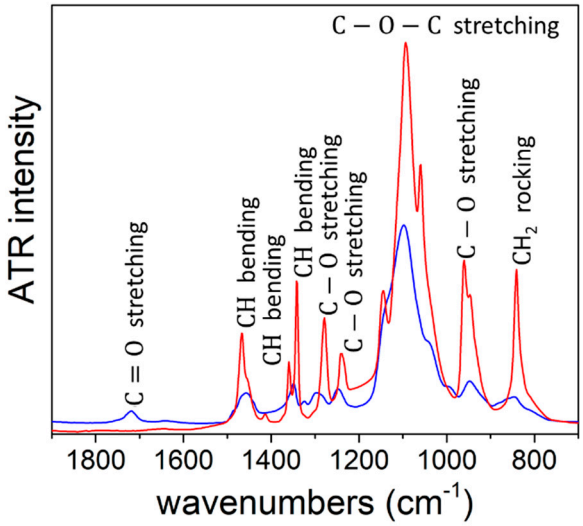

Figure 1. FTIR spectra from uncrosslinked polyethylene oxide (PEO) in the form of PEO powder (red) and crosslinked PEO after drying of swollen and thoroughly washed PEO hydrogels (blue).

In the reaction of PEO with the peroxide the thermal decomposition of Luperox 101 leads to crosslinking by the formation of tertiary alkoxy radicals that abstract the α hydrogens of PEO leading to polyether radicals [13]. Pairs of these radicals may combine to produce ether crosslinks. According to Emami et al. crosslinking may also occur by reaction of the tertiary alkoxy radicals with the polyether radicals which results in acetals with peroxide groups that can also decompose. This may lead to acetal crosslinks with other polyether or acetal radicals. The formed network contains crosslinks that eventually may consist of one ether, two ether, two acetal, or one ether and one acetal linkages [13] (e.g., Scheme 1). Another reaction, that is faster than the one of crosslinking, is between the tertiary alkoxy radicals with the acetal radicals leading to esters. This side-reaction is detected by the peak at 1720 cm^{-1} (Figure 1) implying that the decomposition of Luperox 101 and the production of the radicals that are necessary for crosslinking take place successfully.

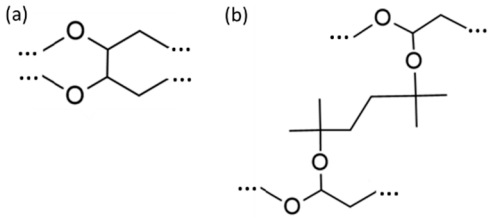

Scheme 1. Possible crosslinking modes of PEO by (**a**) one ether and (**b**) two acetal linkages.

The ability of hydrogels to accommodate large amounts of aqueous media while keeping their mechanical integrity can be proved by swelling experiments. The results from the synthesized hydrogels swollen in water are shown in Table 2. It is found that r_s values are between 400 and 700. The swelling ratio is somewhat higher in hydrogels arising from acetone. There is possibly a slight decrease of r_s as concentration of the crosslinker increases, which would be expected as the molar mass between crosslinks should decrease at higher crosslinker concentrations. However, this drop, although systematic, it is not outside the experimental error.

Table 2. Parameters extracted from swelling experiments.

Parameter/Sample	r_s	ξ_{calc} (nm)	G'_{calc} (Pa)	ρ (10^{23} m^{-3})
AC1	635 ± 52	8.70	573	1.42
AC2	605 ± 45	8.19	628	1.55
AC3	541 ± 65	7.12	780	1.93
BUT1	575 ± 63	7.68	693	1.71
BUT2	548 ± 51	7.24	760	1.88
BUT3	491 ± 41	6.32	938	2.32
DMF1	551 ± 57	7.29	752	1.86
DMF2	556 ± 56	7.37	739	1.83
DMF3	423 ± 37	5.25	1250	3.09

Based on standard theory on swollen networks of neutral hydrophilic polymers one can estimate the correlation length (ξ_{calc}) and the elastic modulus (G'_{calc}) of the PEO hydrogels (Table 2).

$$\frac{1}{\overline{M_c}} = \frac{2}{\overline{M_n}} - \frac{\frac{\bar{v}}{V_1}\left(ln(1-v_2) + v_2 + \chi_1 v_2^2\right)}{v_2^{1/3} - v_2/2} \quad (2)$$

According to Flory–Rehner calculations the molecular weight between crosslinks $\overline{M_c}$ is derived by Equation (2). $\overline{M_n}$ is the number-average molecular weight of the uncrosslinked polymer, V_1 the solvent molar volume, v_2 the volume fraction of the polymer in the swollen hydrogel, $\bar{v}$ the polymer specific volume, and χ_1 the interaction parameter between polymer and solvent [16–20].

The correlation length is written in Equation (3) in terms of the mean-square end-to-end distance of the unperturbed polymer chain $\left(\overline{r_0^2}\right)^{1/2} = lC_n^{1/2}(2n)^{1/2}$ (where l, C_n, and n are the average bond length, polymer characteristic ratio, and number of monomers between crosslinks, respectively). This distance, also termed the characteristic mesh size, is the mean distance between crosslinks in the hydrogel.

$$\xi_{calc} = v_2^{-1/3}\left(\overline{r_0^2}\right)^{1/2} \quad (3)$$

The elastic modulus of the hydrogels is customarily estimated by the average density of crosslinks $\rho = \frac{cN_A}{\overline{M_c}}$ where c is the polymer concentration in the swollen hydrogel (Equation (4)).

$$G'_{calc} = \rho k_B T \quad (4)$$

The estimated correlation length is the average distance between chains segments in the semidilute solution. It is in the order of 5–9 nm and it decreases as crosslinker amount increases. The modulus of the swollen hydrogels is estimated at 600–1200 Pa and (as expected) follows an inverse relation with r_s.

Concentration fluctuations in hydrogels and polymer solutions are traditionally studied by small angle scattering methods where, among others, the correlation length can be measured. Swollen polymer networks differ from uncrosslinked semidilute solutions in terms of morphology because crosslinks introduce spatial concentration fluctuations [21,22] that do not relax by thermal diffusion [23,24]. These static correlations are expressed by a characteristic size (Ξ). Thermal fluctuations that would appear also in uncrosslinked semidilute solutions are present and are expressed by the correlation length of the semidilute solution (ξ). Normally the length-scale of "frozen" correlations is much larger than the solution correlation length ($\Xi \gg \xi$). In literature, a superposition of two scattering functions has been used to model data from swollen hydrogels [21,23–25]. Each of these functions generally consist of a Guinier plateau and a power-law.

In our case SANS data show a low q upturn at $q < 0.01\ A^{-1}$ (Figure 2). Under the assumption of inhomogeneities, this is the power-law regime of the static fluctuations that is dominant at $q \gg 1/\Xi$. Obviously, our SANS measurement window is outside the characteristic length scale of static

fluctuations that originate from the crosslinks. At $q \sim 0.1\ A^{-1}$ the shoulder that appears relates to scattering from semidilute solutions. We used the superposition of two terms (Equations (5)–(7)) i.e., $I_{in}(q)$ and $I_{sd}(q)$ representing inhomogeneities and thermal fluctuations, respectively.

$$I(q) = I_{in}(q) + I_{sd}(q) \tag{5}$$

$$I_{in}(q) = A \cdot q^{-D} \tag{6}$$

$$I_{sd}(q) = B \cdot \left(1 + \left(\frac{d+1}{3}\right) \cdot (q\xi)^2\right)^{-\frac{d}{2}} \tag{7}$$

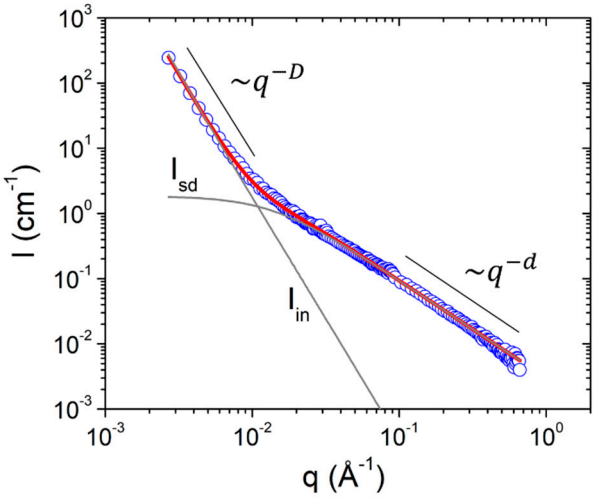

Figure 2. Small angle neutron scattering (SANS) from PEO hydrogel DMF2. Red line is the best fit, gray lines indicate the separate contributions as described in the text. Power-law behaviors are also indicated.

The second term is an empirical function that captures both the correlation length ξ and the characteristic fractal exponent d of the unperturbed chain conformation. This correlation length is a measure of the gel mesh size [26]. The exponents D and d are the characteristic fractal exponent of the inhomogeneities and thermal fluctuations, respectively.

The values of the correlation length ξ measured by SANS (Table 3) are near the ones estimated by swelling experiments (Table 2). In all cases the lowest content of peroxide leads to the highest ξ, however, a systematic decrease of ξ with the increase of crosslinker is clear only in DMF hydrogels. However, in all cases there is a clear and systematic difference between the lowest and the highest amount of crosslinker. Based on the results of Tables 2 and 3 it can be concluded that for all three solvents the mesh size of the PEO networks can be tuned by choosing the proper amount of added peroxide in a range of the order 2–3 nm. The characteristic exponents of the unperturbed segment conformation (d) lie between 1.2 and 1.7 and there is a trend to decrease as crosslinking density increases. This shows a tendency of the PEO segments to change from an excluded volume chain conformation [27,28] (d~1.6) to a more stretched conformation (d~1) as crosslinking density increases. The characteristic exponent of inhomogeneities is about 3.5–3.8 and, therefore, the scattering from these large-scale structures is defined by rough surface fractals.

Table 3. Parameters extracted from small angle neutron scattering (SANS) for the PEO hydrogels.

Parameter/Sample	A (10^{-8} cm^{-1} Å^{-D})	D	B (cm^{-1})	ξ (nm)	d
AC1	12.97	3.67	4.73	10.2	1.69
AC2	45.76	3.46	2.38	6.78	1.57
AC3	9.39	3.80	1.25	8.05	1.18
BUT1	4.16	3.82	4.34	11.9	1.59
BUT2	58.75	3.52	2.01	6.38	1.29
BUT3	10.78	3.71	1.59	7.42	1.35
DMF1	5.57	3.81	4.18	12.3	1.52
DMF2	6.32	3.72	1.85	8.00	1.50
DMF3	4.75	3.84	1.42	7.89	1.25
% δP/P *	3.1	3.5	9.8	8.7	2.0

* uncertainty in parameter estimation.

G′ and G″ from rheology experiments were found fairly frequency-independent while G′ was higher than G″ by roughly an order of magnitude (Figure 3). The measured storage modulus (Table 4) appears not too far from the one estimated from swelling experiments (Table 2). Its values are mostly between 500 and 1000 Pa. There is a tendency of both G′ and G″ to increase as a function of crosslinker percentage which is also followed by the values of ρ (Table 2). However, this trend is very strong in hydrogels synthesized in DMF either in comparison to the other two hydrogels or in comparison to what is expected from swelling experiments. The differences between the hydrogels from different solvents may originate from different degrees of heterogeneity and porosity at the length scale of μm.

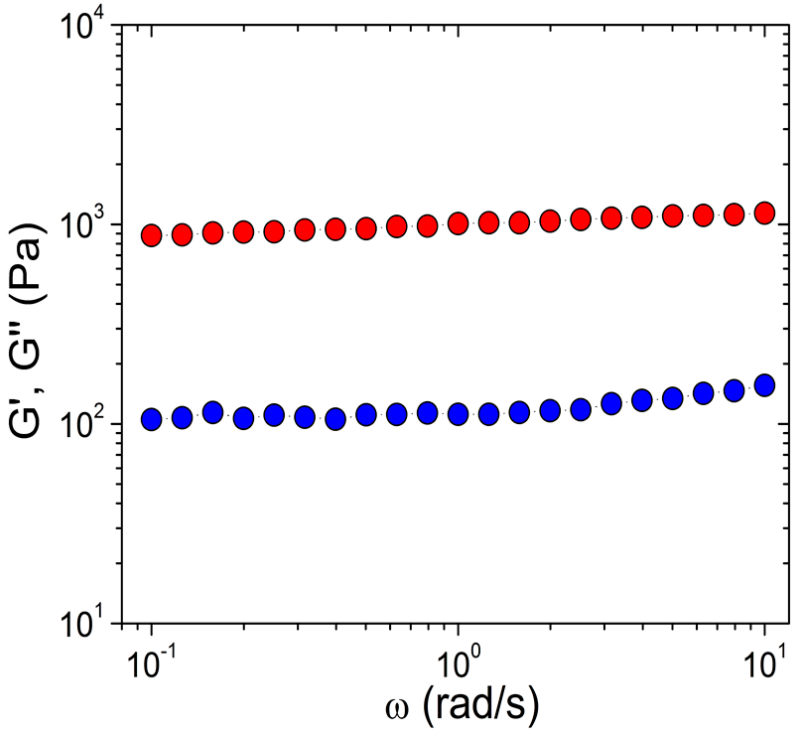

Figure 3. Frequency dependence of storage (G′-red) and loss (G″-blue) modulus from PEO hydrogel AC3.

Table 4. Parameters extracted from rheological experiments.

Parameter/Sample	G′ (Pa)	G″ (Pa)	tan δ
AC1	506	65.2	0.129
AC2	825	74.2	0.090
AC3	1003	119	0.119
BUT1	695	52.0	0.075
BUT2	725	13.4	0.018
BUT3	959	123	0.128
DMF1	251	27.6	0.110
DMF2	902	38.1	0.042
DMF3	1987	170	0.086

The mechanical and swelling properties of the synthesized hydrogels were proved to be adequate for applications in biomaterials for drug delivery and wound healing. The hydrogels are self-supported and can accommodate large amounts of water in order to interact with tissues and cells and at the same time carry growth factors, proteins, and drug molecules. Therefore, we further tested their ability to accommodate and release model globular proteins. Hydrogels originating from AC were chosen for this test because in comparison to DMF and BUT AC has the lowest boiling point. Additionally, it is the solvent proposed in the original works of Emami et al. [13]. The proteins of choice were BSA and LYZ. They have been both used in release studies from PEO hydrogels [16], with BSA being of larger molecular weight and size. The release experiments were performed in water and not in a physiologically relevant medium e.g., PBS because the aim was an investigation that establishes the hydrogels' properties in a range that covers both their fundamental characteristics and their ability to control interactions with biological molecules i.e., from swelling and viscoelasticity to protein diffusion. Therefore, the choice was to do this under conditions that were simplest and uniform for all experiments. In any case no significant electrostatic or specific interaction effects (related with salt ions) are expected in the fairly inert PEO network. The two proteins have different isoelectric points which are about 5 for BSA and 11 for LYZ. Therefore, were expected to have opposite overall charge at pH 6.5 where the experiments were performed. However, only steric and no electrostatic interactions were expected to occur between the proteins and the hydrogel and their charge is not anticipated to change the release properties.

The release of the globular proteins from the hydrogel was modelled by Equation (8). The amount of protein M_t which is released at time t is defined [29] by the amount released at sufficiently long time M_∞ the diffusion coefficient of the protein D within the hydrogel and the hydrogel sample thickness L.

$$\frac{M_t}{M_\infty} = 1 - \sum_{n=0}^{\infty} \frac{8}{(2n+1)^2\pi^2} \cdot exp\left[-\frac{(2n+1)^2\pi^2 D}{L^2}t\right] \quad (8)$$

The release profiles of BSA and LYZ from the hydrogels is illustrated in Figure 4. Data were collected up to 100 h confirming the plateau behavior at long times. However, data up to 50 h are shown for clarity. Fitting with Equation (8) was used to extract the diffusion coefficient of the proteins in the PEO hydrogels. Regarding BSA, the values shown in Table 5 (5–8 $\times 10^{-8}$ cm^2 s^{-1}) are significantly lower than the one of BSA in aqueous media (67 $\times 10^{-8}$ cm^2 s^{-1}). Motion inside the network is hindered as the hydrodynamic radius of BSA [16,30] is 3.5–4 nm and is therefore comparable to the correlation length ξ of the hydrogels. The scaling relation introduced by Lustig and Peppas [31] dictates that the diffusion coefficient D inside the hydrogel will drop in comparison to the one in free solution D_f as $\frac{D}{D_f} = 1 - \frac{R_h}{\xi}$, where R_h is the protein's hydrodynamic radius. A strong decrease of solute diffusivity when the hydrodynamic radius is comparable to the correlation length is also predicted by the more recent scaling [32] and multiscale approach [33]. There is apparently a decrease of D as crosslinker concentration increases (Table 5) which would be expected as ξ was demonstrated to decrease (at least to some extend) by our SANS data (Table 3). Recently mesh size estimation and tuned protein release

were proposed with step growth PEO hydrogels [30]. The authors demonstrated that a delicate tuning of the mesh size allowed the selective release of proteins from a "cocktail" based on their size.

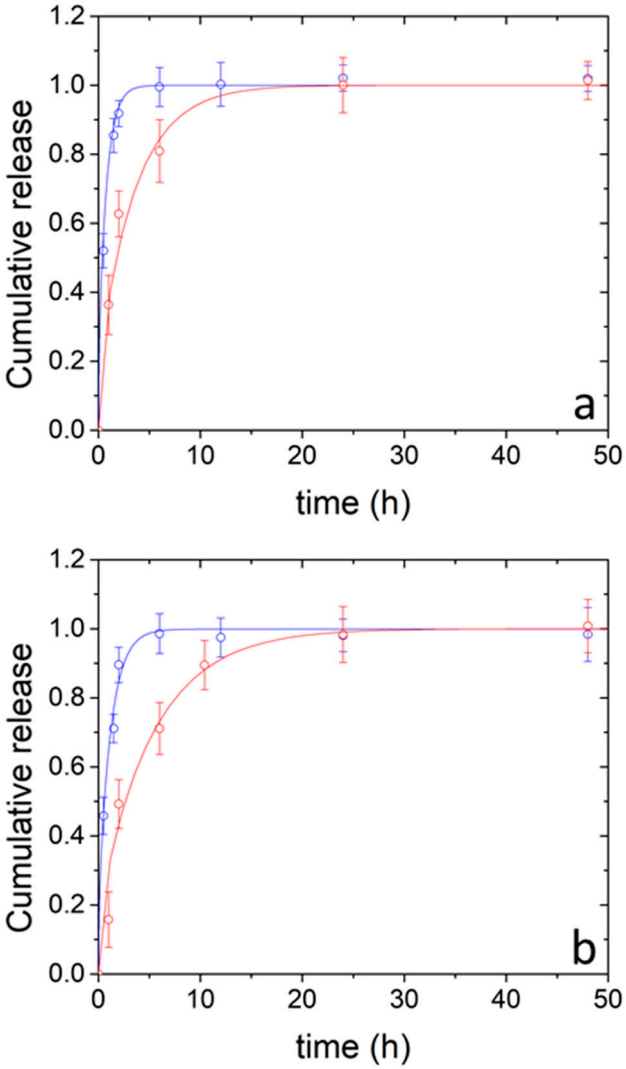

Figure 4. Release profile of bovine serum albumin (BSA) (red) and lysozyme (LYZ) (blue) from hydrogels AC1 (**a**) and AC3 (**b**). Continuous lines are the best fits using Equation (8).

Table 5. Diffusion coefficient (in 10^{-8} cm^2 s^{-1}) of proteins in the hydrogels extracted from release experiments.

Protein/Sample	BSA	LYZ
AC1	7.7 ± 0.8	36 ± 6
AC3	5.2 ± 0.7	24 ± 5

The case of LYZ release (Figure 4) is qualitatively similar to the one in BSA. D is found between 20 and 40 $\times$ 10^{-8} cm^2 s^{-1} whereas for free diffusion of LYZ the value is 145 $\times$ 10^{-8} cm^2 s^{-1}. Although the hydrodynamic radius of LYZ (1.6 nm) is smaller than the one of BSA the effect of the hydrogel on protein's diffusion is evident. It has to be noted that the equilibration time of 144 h allowed for the proteins to load into the hydrogels is adequate. This is evident from Figure 4a,b, where in 40 (BSA) and 20 h (LYZ), respectively, the release kinetics is practically finished. Additionally, the characteristic time for diffusion in (or out) from a hydrogel [34] is $\tau = \frac{L^2}{D}$ which for the slowest diffusion coefficient in this study (5 $\times$ 10^{-8} cm^2 s^{-1}) results to 56 h.

4. Conclusions

Peroxide Luperox 101 was used to prepare PEO hydrogels in the melt by the thermally stimulated tertiary alkoxy radicals and abstraction of α hydrogens of PEO. This versatile synthesis scheme allows fabrication of hydrogels with mesh size in the order of the size of globular proteins (≈10 nm) and modulus between 500 and 1000 Pa. Swelling experiments in water were predictive of the mesh size and modulus of the hydrogels and they were supported by SANS and rheometry. The mesh size of the hydrogels could be tuned by the peroxide content. The diffusion of the model proteins BSA and LYZ from the hydrogels was found slower for BSA in comparison to LYZ because of their different sizes. Additionally, it was demonstrated that protein release profiles correlated with the mesh size of the prepared networks. Therefore, these hydrogels can be designed as platforms for controllable release of biomacromolecules.

Author Contributions: Conceptualization, A.P. and E.V.; methodology, A.P., E.V. and A.R.; software, A.P. and A.R.; validation, A.P., E.V. and A.R.; formal analysis, A.P., E.V. and A.R.; investigation, A.P., E.V. and A.R.; resources, A.P., E.V., S.P., C.T., and A.R.; data curation, A.P., E.V., S.P., C.T. and A.R.; writing—original draft preparation, A.P. and E.V.; writing—review and editing, A.P., E.V., S.P., C.T. and A.R.; visualization, A.P., E.V. and A.R.. All authors have read and agreed to the published version of the manuscript.

Funding: This research received no external funding.

Acknowledgments: This work is based upon experiments performed at the KWS-2 instrument operated by JCNS at the Heinz Maier-Leibnitz Zentrum (MLZ), Garching, Germany.

Conflicts of Interest: The authors declare no conflict of interest.

References

1. Schwall, C.T.; Banerjee, I.A. Micro- and Nanoscale Hydrogel Systems for Drug Delivery and Tissue Engineering. *Materials* **2009**, *2*, 577–612. [CrossRef]
2. D'souza, A.A.; Shegokar, R. Polyethylene glycol (PEG): A versatile polymer for pharmaceutical applications. *Expert Opin. Drug Deliv.* **2016**, *13*, 1257–1275. [CrossRef]
3. Tong, X.; Lee, S.; Bararpour, L.; Yang, F. Long-Term Controlled Protein Release from Poly(Ethylene Glycol) Hydrogels by Modulating Mesh Size and Degradation. *Macromol. Biosci.* **2015**, *15*, 1679–1686. [CrossRef] [PubMed]
4. Zia, F.; Anjum, M.N.; Saif, M.J.; Jamil, T.; Malik, K.; Anjum, S.; BiBi, I.; Zia, M.A. Chapter 16–Alginate-Poly(Ethylene) Glycol and Poly(Ethylene) Oxide Blend Materials. In *Algae Based Polymers, Blends, and Composites*; Zia, K.M., Zuber, M., Ali, M., Eds.; Elsevier: Amsterdam, The Netherlands, 2017; pp. 581–601. [CrossRef]
5. Whitehead, A.K.; Barnett, H.H.; Caldorera-Moore, M.E.; Newman, J.J. Poly(ethylene glycol) hydrogel elasticity influences human mesenchymal stem cell behavior. *Regen. Biomater.* **2018**, *5*, 167–175. [CrossRef] [PubMed]
6. Chen, S.-L.; Fu, R.-H.; Liao, S.-F.; Liu, S.-P.; Lin, S.-Z.; Wang, Y.-C. A PEG-Based Hydrogel for Effective Wound Care Management. *Cell Transpl.* **2018**, *27*, 275–284. [CrossRef] [PubMed]
7. Yamaguchi, N.; Kiick, K.L. Polysaccharide-poly(ethylene glycol) star copolymer as a scaffold for the production of bioactive hydrogels. *Biomacromolecules* **2005**, *6*, 1921–1930. [CrossRef] [PubMed]
8. Lee, S.Y.; Bang, S.; Kim, S.; Jo, S.Y.; Kim, B.-C.; Hwang, Y.; Noh, I. Synthesis and in vitro characterizations of porous carboxymethyl cellulose-poly(ethylene oxide) hydrogel film. *Biomater. Res.* **2015**, *19*, 12. [CrossRef]
9. Wei, L.; McDonald, A.G. Peroxide induced cross-linking by reactive melt processing of two biopolyesters: Poly(3-hydroxybutyrate) and poly(l-lactic acid) to improve their melting processability. *J. Appl. Polym. Sci.* **2015**, *132*, 41724. [CrossRef]
10. Takamura, M.; Nakamura, T.; Kawaguchi, S.; Takahashi, T.; Koyama, K. Molecular characterization and crystallization behavior of peroxide-induced slightly crosslinked poly(L-lactide) during extrusion. *Polym. J.* **2010**, *42*, 600–608. [CrossRef]
11. Liu, S.-Q.; Gong, W.-G.; Zheng, B.-C. The Effect of Peroxide Cross-Linking on the Properties of Low-Density Polyethylene. *J. Macromol. Sci. Part B* **2014**, *53*, 67–77. [CrossRef]

12. Jiang, Q.; Li, J.; Huang, W.; Zhang, D.; Chen, J.; Yang, H.; Xue, X.; Jiang, B. Radical polymerization in the presence of a peroxide monomer: An approach to branched vinyl polymers. *Polym. Chem.* **2017**, *8*, 4428–4439. [CrossRef]
13. Emami, S.H.; Salovey, R.; Hogen-Esch, T.E. Peroxide-mediated crosslinking of poly(ethylene oxide). *J. Polym. Sci. Part A Polym. Chem.* **2002**, *40*, 3021–3026. [CrossRef]
14. Emami, S.H.; Salovey, R.; Hogen-Esch, T.E. Degradable poly(ethylene oxide) hydrogels formed by crosslinking with tert-butylperoxybenzoate. *J. Polym. Sci. Part A Polym. Chem.* **2003**, *41*, 520–527. [CrossRef]
15. Lin, C.-C.; Anseth, K.S. Controlling Affinity Binding with Peptide-Functionalized Poly(ethylene glycol) Hydrogels. *Adv. Funct. Mater.* **2009**, *19*, 2325–2331. [CrossRef]
16. Zustiak, S.P.; Leach, J.B. Characterization of protein release from hydrolytically degradable poly(ethylene glycol) hydrogels. *Biotechnol. Bioeng.* **2011**, *108*, 197–206. [CrossRef]
17. Barker, J.G.; Pedersen, J.S. Instrumental Smearing Effects in Radially Symmetric Small-Angle Neutron Scattering by Numerical and Analytical Methods. *J. Appl. Crystallogr.* **1995**, *28*, 105–114. [CrossRef]
18. Radulescu, A.; Szekely, N.K.; Polachowski, S.; Leyendecker, M.; Amann, M.; Buitenhuis, J.; Drochner, M.; Engels, R.; Hanslik, R.; Kemmerling, G.; et al. Tuning the instrument resolution using chopper and time of flight at the small-angle neutron scattering diffractometer KWS-2. *J. Appl. Crystallogr.* **2015**, *48*, 1849–1859. [CrossRef]
19. Vad, T.; Sager, W.F.C.; Zhang, J.; Buitenhuis, J.; Radulescu, A. Experimental determination of resolution function parameters from small-angle neutron scattering data of a colloidal SiO_2 dispersion. *J. Appl. Crystallogr.* **2010**, *43*, 686–692. [CrossRef]
20. Zustiak, S.P.; Leach, J.B. Hydrolytically Degradable Poly(Ethylene Glycol) Hydrogel Scaffolds with Tunable Degradation and Mechanical Properties. *Biomacromolecules* **2010**, *11*, 1348–1357. [CrossRef]
21. Horkay, F.; McKenna, G.B.; Deschamps, P.; Geissler, E. Neutron Scattering Properties of Randomly Cross-Linked Polyisoprene Gels. *Macromolecules* **2000**, *33*, 5215–5220. [CrossRef]
22. Panyukov, S.; Rabin, Y. Polymer Gels: Frozen Inhomogeneities and Density Fluctuations. *Macromolecules* **1996**, *29*, 7960–7975. [CrossRef]
23. Shibayama, M. Small-angle neutron scattering on polymer gels: Phase behavior, inhomogeneities and deformation mechanisms. *Polym. J.* **2011**, *43*, 18–34. [CrossRef]
24. Shibayama, M.; Kurokawa, H.; Nomura, S.; Muthukumar, M.; Stein, R.S.; Roy, S. Small-angle neutron scattering from poly(vinyl alcohol)-borate gels. *Polymer* **1992**, *33*, 2883–2890. [CrossRef]
25. Papagiannopoulos, A. Chapter 10—Small-Angle Neutron Scattering (SANS). In *Microscopy Methods in Nanomaterials Characterization*; Thomas, S., Thomas, R., Zachariah, A.K., Mishra, R.K., Eds.; Elsevier: Amsterdam, The Netherlands, 2017; pp. 339–361. [CrossRef]
26. Saffer, E.M.; Lackey, M.A.; Griffin, D.M.; Kishore, S.; Tew, G.N.; Bhatia, S.R. SANS study of highly resilient poly(ethylene glycol) hydrogels. *Soft Matter.* **2014**, *10*, 1905–1916. [CrossRef]
27. Schaefer, D.W.; Rieker, T.; Agamalian, M.; Lin, J.S.; Fischer, D.; Sukumaran, S.; Chen, C.; Beaucage, G.; Herd, C.; Ivie, J. Multilevel structure of reinforcing silica and carbon. *J. Appl. Crystallogr.* **2000**, *33*, 587–591. [CrossRef]
28. Schmidt, P.W. Small-angle scattering studies of disordered, porous and fractal systems. *J. Appl. Crystallogr.* **1991**, *24*, 414–435. [CrossRef]
29. Lin, C.-C.; Metters, A.T. Hydrogels in controlled release formulations: Network design and mathematical modeling. *Adv. Drug Deliv. Rev.* **2006**, *58*, 1379–1408. [CrossRef]
30. Rehmann, M.S.; Skeens, K.M.; Kharkar, P.M.; Ford, E.M.; Maverakis, E.; Lee, K.H.; Kloxin, A.M. Tuning and Predicting Mesh Size and Protein Release from Step Growth Hydrogels. *Biomacromolecules* **2017**, *18*, 3131–3142. [CrossRef]
31. Lustig, S.R.; Peppas, N.A. Solute diffusion in swollen membranes. IX. Scaling laws for solute diffusion in gels. *J. Appl. Polym. Sci.* **1988**, *36*, 735–747. [CrossRef]
32. Hadjiev, N.A.; Amsden, B.G. An assessment of the ability of the obstruction-scaling model to estimate solute diffusion coefficients in hydrogels. *J. Control. Release* **2015**, *199*, 10–16. [CrossRef]
33. Axpe, E.; Chan, D.; Offeddu, G.S.; Chang, Y.; Merida, D.; Hernandez, H.L.; Appel, E.A. A Multiscale Model for Solute Diffusion in Hydrogels. *Macromolecules* **2019**, *52*, 6889–6897. [CrossRef] [PubMed]

34. Weber, L.M.; Lopez, C.G.; Anseth, K.S. Effects of PEG hydrogel crosslinking density on protein diffusion and encapsulated islet survival and function. *J. Biomed. Mater. Res. Part A* **2009**, *90A*, 720–729. [CrossRef] [PubMed]